Geoderma 213 (2014) 15–28

Contents lists available at ScienceDirect

Geoderma

journal homepage: www.elsevier.com/locate/geoderma

Digital mapping of soil salinity in Ardakan region, central Iran

R. Taghizadeh-Mehrjardi [a,*], B. Minasny [b], F. Sarmadian [c], B.P. Malone [b]

[a] Faculty of Agriculture and Natural Resources, University of Ardakan, P.O. Box 89516-56767, Yazd, Iran
[b] Soil Security Laboratory, Faculty of Agriculture & Environment, The University of Sydney, NSW 2006 Australia
[c] Faculty of Agricultural Engineering and Technology, University College of Agriculture and Natural Resources, University of Tehran, P.O. Box 31587-77871, Karaj, Iran

ARTICLE INFO

Article history:
Received 10 October 2012
Received in revised form 27 June 2013
Accepted 21 July 2013
Available online 23 August 2013

Keywords:
Digital soil mapping
Soil salinity
Regression tree analysis
Apparent electrical conductivity

ABSTRACT

Salinization and alkalinization are the most important land degradation processes in central Iran. In this study we modelled the vertical and lateral variation of soil salinity (measured as electrical conductivity in saturation paste, ECe) using a combination of regression tree analysis and equal-area smoothing splines in a 72,000 ha area located in central Iran. Using the conditioned Latin hypercube sampling method, 173 soil profiles were sampled from the study area, and then analysed for ECe and other soil properties. Auxiliary data used in this study to represent predictive soil forming factors were terrain attributes (derived from a digital elevation model), Landsat 7 ETM$^+$ data, apparent electrical conductivity (ECa)—measured using an electromagnetic induction instrument (EMI), and a geomorphologic surfaces map. To derive the relationships between ECe (from soil surface to 1 m) and the auxiliary data, regression tree analysis was applied. In general, results showed that the ECa surfaces are the most powerful predictors for ECe at three depth intervals (i.e. 0–15, 15–30 and 30–60 cm). In the 60–100 cm depth interval, topographic wetness index was the most important parameter used in regression tree model. Validation of the predictive models at each depth interval resulted in R^2 values ranging from 78% (0–15 cm) to 11% (60–100 cm). Thus we can recommend similar applications of this technique could be used for mapping soil salinity in other parts in Iran.

1. Introduction

Salinization and alkalinization are the most important land degradation processes in central Iran. In these areas, soluble salts accumulate in the soil, resulting into a gradual decline in crop production (Farifteh et al., 2006). In recent years, the production of pistachio in Yazd province, the second most important region for pistachio cultivation in central of Iran, has decreased dramatically due to increasing soil salinity. Therefore, to manage this problem, detailed knowledge about the spatial distribution of soil salinity is needed.

There are various legacy soil maps in Iran that were produced based on traditional approaches. This information is impractical for quantitative studies due to its qualitative nature. Furthermore, the scale at which the soil information is available is often too coarse and impractical for detailed understanding of soil variation, particularly for agricultural soil management at the farm and field scales. To overcome some of these limitations, the application of digital soil mapping (DSM) techniques is seen as an efficient alternative approach (McBratney et al., 2003). This is because the underlying principle in DSM is to use computer assisted methods to derive comprehensive soil-landscape relationships using sparsely observed soil data with detailed and readily available auxiliary variables in an objective way. This study will use a range of contemporary digital mapping techniques to map the vertical and lateral variation of soil salinity (90 m × 90 m × 0.1 m) in a 72,000 ha area in the Ardakan region in central Iran.

The first requirement in DSM is the compilation of auxiliary or *scorpan* (McBratney et al., 2003) variables for the prediction of soil salinity parameters. These include remote sensing data, topographical variables (derived from a digital elevation model), apparent electrical conductivity and soil type information. For example, studies that have exclusively used topographic variables include Metternicht and Zinck (1997) and Sheng et al. (2010). Douaoui et al. (2006), Alavi-panah and Goossens (2001), Dehni and Lounis (2012) and Bouaziz et al. (2011) relied exclusively on remote sensing data for understanding the spatial distribution of soil salinity. Mapping with a combination of both topographical and remote sensing variables was investigated by Evans and Caccetta (2000) and Bilgili (2013). In addition to this, some researchers have considered the use of apparent electrical conductivity (ECa) derived using proximal sensor platforms such as the Geonics electromagnetic induction (EMI), as an easy-to-obtain ancillary information source to map soil properties (Michot et al., 2013; Sun et al., 2012, 2013). Good relationships between soil salinity and ECa values have been reported by Lesch et al. (2005), Triantafilis et al. (2001), and Triantafilis and Lesch (2005).

McBratney et al. (2003) described various modelling techniques used in DSM studies. Some of these include multiple linear regression, artificial neural networks (Akramkhanov and Vlek, 2012), and machine learning systems and data mining algorithms (Lacoste et al., 2011). Hybrid modelling approaches such as regression kriging (Hengl et al.,

* Corresponding author. Tel.: +98 3527220911; fax: +98 3527226767.
E-mail address: rh_taghizade@yahoo.com (R. Taghizadeh-Mehrjardi).

0016-7061/$ – see front matter © 2013 Elsevier B.V. All rights reserved.
http://dx.doi.org/10.1016/j.geoderma.2013.07.020

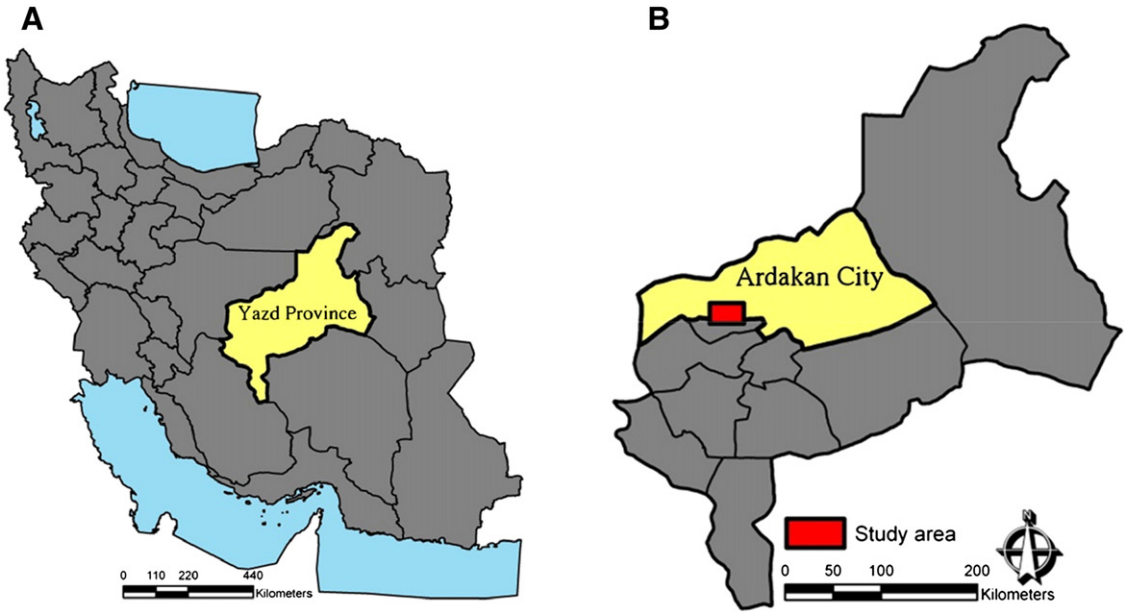
A
Yazd Province
0 110 220 440
Kilometers
B
Ardakan City
Study area
0 50 100 200
Kilometers

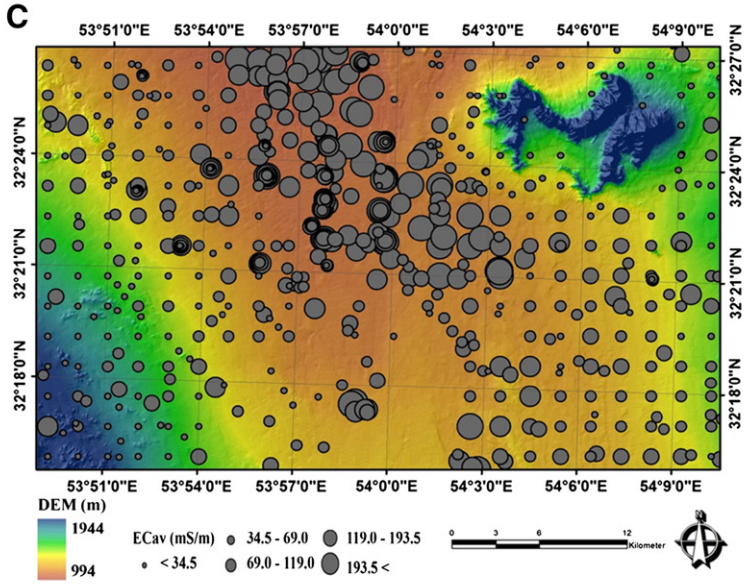
C
53°51'0"E
53°54'0"E
53°57'0"E
54°0'0"E
54°3'0"E
54°6'0"E
54°9'0"E
32°27'0"N
32°24'0"N
32°21'0"N
32°18'0"N
DEM (m)
1944
994
ECav (mS/m)
< 34.5
34.5 - 69.0
69.0 - 119.0
119.0 - 193.5
193.5 <
0 3 6 12
Kilometer

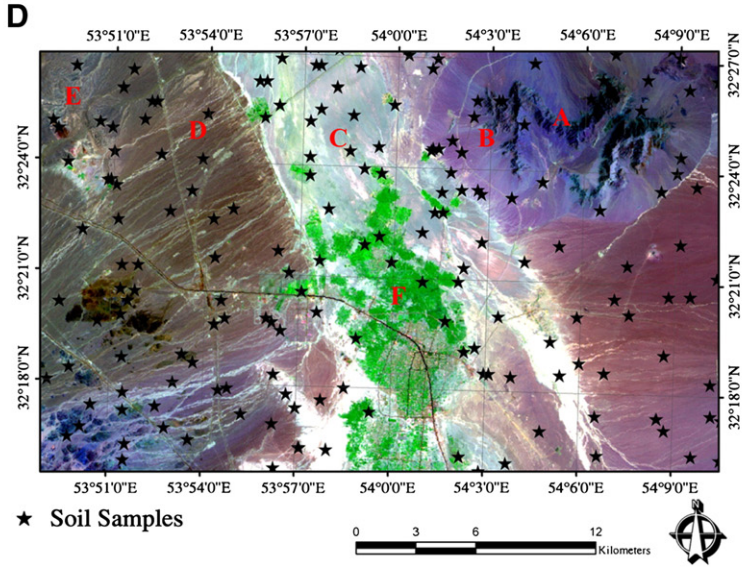
D
53°51'0"E
53°54'0"E
53°57'0"E
54°0'0"E
54°3'0"E
54°6'0"E
54°9'0"E
32°27'0"N
32°24'0"N
32°21'0"N
32°18'0"N
E
D
C
B
A
F
★ Soil Samples
0 3 6 12
Kilometers

2004; Michot et al., 2013; Vanwalleghem et al., 2010; Vasques et al., 2010) are also used frequently in the DSM community. Another form of data mining is the regression or decision tree analysis and their variants (Florinsky et al., 2002; Ließ et al., 2012; Mendonça-Santos et al., 2006; Ryan et al., 2000; Vasques et al., 2010). Decision trees are non-parametric (i.e. no assumptions about variable distribution) nor are they sensitive to missing data (Bui et al., 1999; Moran and Bui, 2002). Also, they select the most relevant variable subsets for modelling. Another advantage of decision tree analysis is their ease of interpretation and their ability to incorporate both continuous and categorical auxiliary data (Grinand et al., 2008); which would make using this type of modelling approach suitable in places such as Iran.

Most studies only produce digital soil salinity maps for specific depth intervals. However, as commonly accepted, soil salinity generally varies continuously within a profile. This variation can be modelled using continuous soil depth functions (Malone et al., 2009). Several researchers have attempted to derive some functions of soil variation with depth, for example Jenny (1941), Minasny et al. (2006), Mishra et al. (2009), and Kempen et al. (2011). Added to this, Bishop et al. (1999) also compared different depth functions to predict some soil properties including soil pH, electrical conductivity, clay content, organic carbon content and water content and they found that equal-area splines were the most flexible and practicable depth functions. An amalgam of fitting the spline depth function and DSM was demonstrated by Malone et al. (2009) whom mapped to 1 m, the vertical and lateral variation of carbon storage and available water capacity across an area in the northwestern NSW, Australia. Given the range of contemporary methods used in mapping the vertical and lateral variation of soil properties, no attempt has been presented to use the spline depth function and DSM techniques, to predict and map salinity level in an arid region. Therefore, we attempt to investigate soil salinity variation in these spatial domains for a study area within Iran.

2. Materials and methods

2.1. Study area

The study area is the Ardakan region in Yazd province located in central Iran (Fig. 1a). It covers an area of 72,000 ha (Fig. 1b). The predominant crops have been cultivated in the plain are pistachio nuts, followed by wheat and madder (*Rubia tinctorum* L.). The climate of the study area is arid with a mean annual precipitation, mean annual temperature, and annual potential evaporation of 75 mm, 18.5 °C, and 3483 mm, respectively. Precipitation is very rare and received mainly during the winter season. The soil moisture and temperature regimes are aridic and thermic, respectively. Topography of the land is flat, and the maximum elevation of the region is 1944 m.a.s.l. (metres above sea level) and the minimum elevation is 944 m.a.s.l. (Fig. 1c). The major geological units are composed of red gypsiferous marls and brown to grey limestone, and the main landforms of the region from east to west direction are alluvial fans, coalescing alluvial fans (bajadas), salt plain and gypsiferous hills, respectively (Fig. 1d). The soils in the study area have been classified using the US Soil Taxonomy (Soil Survey Staff, 2006) into two orders (i.e. Aridisols and Entisols), five sub-orders (i.e. Calcids, Cambids, Gypsids, Salids and Orthents), six great groups (i.e. Haplocalcids, Haplocambids, Calcigypsids, Haplogypsids, Haplosalids and Torriorthents) and eight sub-great groups (i.e. Typic Haplocalcids, Typic Haplocambids, Typic Calcigypsids, Typic Haplogypsids, Typic Haplosalids, Petrogypsic Haplosalids, Gypsic Haplosalids and Typic Torriorthents). In general, soils found in the upper land (Fig. 1c) have coarse texture and low salinity (loamy sandy to sandy clay loamy), while soils characterised with more saline and fine texture are located in lower part of the area (clay loam to clay). Soils have low amount of soil organic matter (ranges from 0.01 to 0.9%) and high amount of $CaCO_3$ (14 to 40%) and gypsum (2 to 45%).

2.2. Procedures

The flowchart of this study, shown in Fig. 2, illustrates the procedures employed in this research.

This work is conducted in a number of stages:

i) Collecting soil samples for calibration based on Latin hypercube sampling;
ii) Fitting of equal-area smoothing spline functions to soil electrical conductivity (ECe) at the point observations;
iii) Preparing of *scorpan* variables at a regular grid spacing, and intersecting the variables with the point observations;
iv) Creating digital maps of apparent electrical conductivity (ECa) based on electrical magnetic induction measurement and *scorpan* variables;
v) Deriving empirical relationships of ECe with the available *scorpan* variables using the regression rule model; and
vi) Applying the models to the entire study area in order to produce a soil salinity map with the intended purpose of it being used for local agricultural soil management.

Michot et al. (2013) recently mapped soil salinity in an 8 ha rice field in the Niger. The data collected were similar to this study (140 ECe observations, and 423 ECa measurements), but they applied a different method. They first modelled ECe as a function of ECa using a regression tree. Then they predicted ECe on the observed ECa locations, and mapped ECe at a regular grid at 3 different depths using ordinary kriging.

2.3. Acquisition of auxiliary data

Digital soil mapping relies on the empirical relationship between soil properties and their environmental factors—that is, soil, climate, organisms, relief, parent materials and spatial position (McBratney et al., 2003). Upon both an understanding of the factors which may affect soil salinity distribution and availability of such spatial environmental information, four types of auxiliary data were available in this study area (Table 1), and include:

2.3.1. Terrain attributes

The role of land surface parameters in soil mapping has been reviewed by McKenzie et al. (2000). However, relief in flat areas could well be explained by using terrain attributes such as those developed by Gallant and Dowling (2003) that include Multi-resolution Valley Bottom Flatness (MrVBF), which as the name implies, is a multi-scale algorithm for identifying and classifying the degrees of valley bottom flatness from a DEM, into a single index. Other attributes include valley depth (Abdel-Kader, 2011), elevation, altitude above channel network, modified catchment area and mid-slope position (Bohner and Antonic, 2009). Furthermore, topographic wetness index, indicating the degree of wetness and hydrology of the landscape has previously been used to classify areas with saline soils (Moore et al., 1991). Also, in order to capture subsurface soil moisture flow, catchment slope has been found to be useful (Scull et al., 2005).

All terrain attributes used in this study were derived from a DEM with a 10 m grid resolution (National Cartographic Center, 2010). From Fig. 1c, it is clear that most of the study area has low elevation and, is dominantly flat. Since soils in flat areas are not dominantly

Fig. 1. (a) Location of the Yazd province, (b) the Ardakan region, and the study area in central Iran and (c) ECa site data locations draped over digital elevation model and (d) spatial distribution of soil samples draped over the ETM^+ image (A: Mountain landscape with rock surfaces, B: Alluvial fan, C: Playa, with fine and to some extent coarse alluvial sediment, D: coalescing alluvial fans (bajadas), E: gypsiferous hills, F: Pistachio orchard).

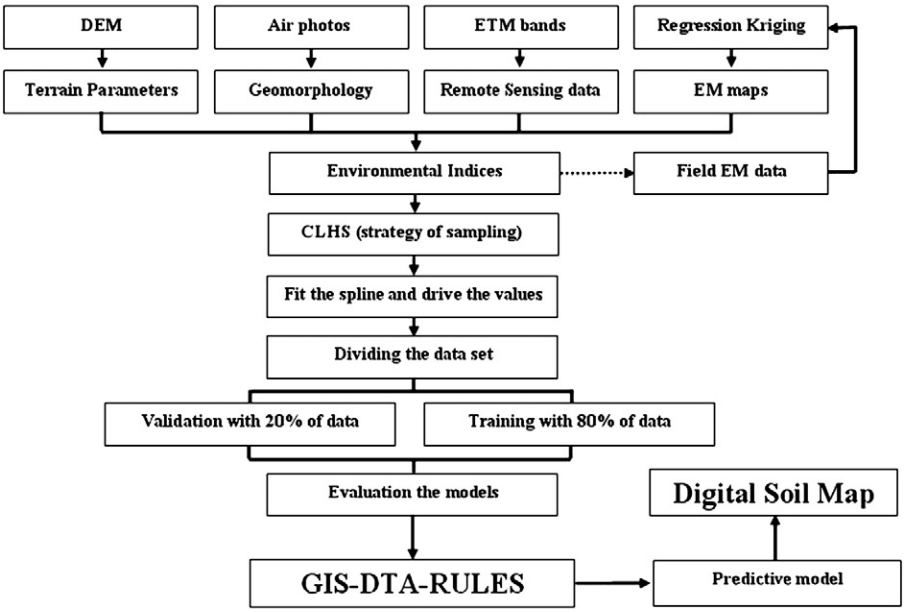

Fig. 2. Flowchart of methodology used for digital soil mapping in this study.

influenced by local topographic characteristics, we did not consider local terrain attributes such as slope and curvatures (Scull et al., 2005).

The DEM used in this study was originally prepared from RADAR images (National Cartographic Center, 2010). The raw DEM contains a number of anomalies—and by all accounts, is a 'noisy' dataset—as a result of the data collection and method of preparation. This in turn affects the derivation of the terrain attributes from the DEM. Therefore, in this study, we used the wavelet analysis for removing noise and understanding the scale dependent behaviour of the terrain attributes. As has been previously found, one of the best methods for decomposing data into different scale components is wavelet functions (Graps, 1995). Wavelets are useful for analysing data with sharp discontinuities (Lark and McBratney, 2002) and also effective in removing redundant information from data layers (Mendonça-Santos et al., 2006). Wavelet partitions data into different frequency components, this allows us to study each of the components with a resolution matched to its scale. Therefore, a two-dimensional discrete wavelet transform in MATLAB software (MathWorks, 2010) was used to decompose the terrain attribute layers (Lark and Webster, 2004) and remove the noises and artefacts. The terrain attribute data layers were decomposed into four levels: L1, L2, L3 and L4. These levels corresponded to grid resolutions of 20, 40, 80, and 160 m respectively.

2.3.2. Remote sensing data

Most of our study area is bare land; hence variation of soil properties/types at the terrain surface can be detected by remote sensing data (Metternicht and Zinck, 2003). This is because different soils variably absorb and/or reflect electromagnetic radiation at different wavelengths (Andronikov and Dorbrolv'skiy, 1991). A Landsat 7 ETM^{+} image acquired on August 2002 was used in this study. It consists of six spectral bands (B1 (0.45–0.52 μm), B2 (0.52–0.60 μm), B3 (0.63–0.69 μm), B4 (0.76–0.90 μm), B5 (1.55–1.75 μm) and B7 (2.08–2.35 μm)), and has a grid resolution of approximately 30 m. To reduce the total number of data layers, a principal component analysis (PCA) based on its correlation matrix was used. Metternicht and Zinck (2003) and similarly, Dwivedi and Sreenivas (1998) demonstrated that PCA based on correlation matrix is an effective approach to discriminate soils in arid regions. Also, according to pedogenesis of the soils at the study area, other indices were also computed, which included Normalized Difference Vegetation Index (NDVI)—an index of vegetation distribution and density. In addition, clay index, carbonate index, gypsum index, salinity index and brightness index were also derived from the ETM^{+} bands in order to differentiate the geologic composition of surficial materials (see the definition of the indices in Table 1).

2.3.3. Geomorphology map

A useful source of information for assessing soil parent material and other factors of soil genesis, particularly in arid areas is the use of geomorphology maps (Jafari et al., 2012; Scull et al., 2005). For this study, a geomorphology map was prepared based on a nested geomorphic hierarchy approach defined by Toomanian et al. (2006). In this approach, air photos (1:50,000) were used to delineate geomorphological entities into four levels which included: landscape, landform, lithology and geomorphological surface. After ortho-photo geo-referencing of aerial photos, delineated boundaries of geomorphological surfaces were inserted in a GIS environment. This study area has 25 geomorphological units (Fig. 3a and Table 2).

All data sources that have been described were registered to a common grid of 30 m cell size.

2.3.4. Apparent electrical conductivity

An additional analysis in this study was mapping the apparent electrical conductivity (ECa) of the bulk soil as a means for predicting ECe across the study area. ECa was measured using the electromagnetic induction instrument (EMI, Geonics EM38). The device measures ECa in two modes: vertical (ECav) and horizontal (ECah)—working to effective depths of 1.5 m and 0.75 m respectively (Sun et al., 2013). In order to generate ECa maps efficiently for the study area, field ECa data were collected in different campaigns. The first of which were 173 ECa readings taken at the sites used for the soil sampling. These data were also used to investigate the calibration of ECa data with ECe measurements at these sites. An additional 216 ECa readings were taken from 24 transects. These transect were selected randomly and in each, nine ECa readings were taken with the mean distance 30 m. A further 311 readings were gathered based on a grid sample with mean distance of 1500 m between sites in order to adequately cover the study area (Fig. 1c). In total, 700 ECa data in both vertical and horizontal modes were taken for this study.

Spatial prediction and mapping of the ECa data was performed using local regression kriging. For each mode of ECa measurement, regression trees, facilitated through the Cubist data mining software (Quinlan, 2001), modelled the deterministic spatial trend. Auxiliary

Table 1
Land surface parameters used for spatial prediction of soil ECe.

Auxiliary data	Land surface parameters	Definition	Reference/source	Soil forming factors
Apparent electrical conductivity	ECa readings	Calculated the ECa of soil volume down to 1.5 m	Geonics Ltd. EM38	S, PM
Terrain attributes	Elevation	Height above sea level (m)	National Cartographic Center (2010)	R
	Altitude above channel network	Relative height above depth	SAGA GIS	R
	Modified catchment area	Calculated the flow accumulation and related parameters	SAGA GIS	R
	Mid-slope position	Calculates the extent that each point similar to a ridge or valley position as values 0 through 100	Bohner and Antonic (2009)	R
	Multi-resolution Ridge-top Flatness Index (MrRTF)	Measure of flatness and lowness	Gallant and Dowling (2003)	R
	Multi-resolution Valley Bottom Flatness Index (MrVBF)	Measure of flatness and upness	Gallant and Dowling (2003)	R
	Valley depth	Metres	SAGA GIS	R
	Topographic wetness index	Ln (FA/SG)	SAGA GIS	R, CL
	Catchment slope (CS)	Average gradient above flow path	SAGA GIS	R, CL
Remote sensing data	Principal components of six ETM bands	PC1, PC2, PC3	Nield et al. (2007)	PM, S, T
	Normalized Difference Vegetation Index (NDVI)	(B4 − B3)/(B4 + B3)	Boettinger et al. (2008)	O
	Clay index	B5/B7	Boettinger et al. (2008)	PM, S
	Gypsum index	(B5 − B4)/(B5 + B4)	Nield et al. (2007)	PM, S
	Salinity ratio	(B3 − B4)/(B2 + B4)	Metternicht and Zinck (2003)	PM, S
	Brightness index	$((B3)^2 + (B4)^2)^{0.5}$	Metternicht and Zinck (2003)	PM, S
	Carbonate index	B3/B2	Boettinger et al. (2008)	PM, S
Geomorphology	Geomorphology map	Geomorphology surfaces	Toomanian et al. (2006)	PM, S, T

R: Relief, CL: Climate, PM: Parent materials, S: Soil, and T: Time.

data (i.e. ETM$^+$ images, geomorphology, and terrain parameters) were used as covariates to model this spatial trend. Kriging with local variograms of the residuals (resulting from the regression tree model) was performed to capture the stochastic variation of the spatial model through the Vesper software (Minasny et al., 1999). Calibration of the predictive models was based on using a random sample of 80% of the available data. And the remaining 20% of the data is used as validation.

2.4. Data collection and soil sample analysis

A sampling campaign was conducted in which 173 individual sites were visited and soil was sampled. The configuration of the sampling locations was based on the conditioned Latin hypercube method (Minasny and McBratney, 2006) using a number of environmental variables that were found to have the most variation within the area. These included: (from a DEM) LS factor, stream power index, slope length, slope, and aspect. Geomorphologic units and data from the Landsat ETM$^+$ (2002), specifically the spectral bands 3, 4, 5 and 7 were also included. Fig. 1d shows the location of the soil profiles draped over the Landsat ETM$^+$ image.

At each site, soil samples were collected based on their genetic horizons. Overall, 598 soil samples were taken and then transported to laboratory. The samples were air-dried at room temperature, ground to pass through a 2-mm sieve prior to analysis (Sparks et al., 1996). Particle size distribution, electrical conductivity (ECe), pH, organic carbon, soluble calcium, magnesium, chlorine, carbonate, bicarbonate, sodium, potassium were measured according to standard methods (Nelson and Sommers, 1982; Sparks et al., 1996). Also, sodium absorption ratio (SAR) was calculated according to the equation defined by Suarez (1981).

In order to describe the vertical variation of ECe, we standardise the depth intervals of prediction: 0–15, 15–30, 30–60 and 60–100 cm. Harmonisation (to the standard depths) of the raw soil profile ECe data was performed using the equal-area quadratic spline model described in Malone et al. (2009). We fitted the spline function to each profile to a maximum depth of 1 m. Integration of the splines to the defined depth intervals was performed to obtain values of ECe at the standardised depths for each soil profile.

2.5. Spatial prediction of ECe and validation

A regression tree correlates several covariates with direct or indirect relationships to a target variable with a tree structure, generated by partitioning the data recursively into a number of groups. A constructed regression tree consists of nodes (each representing an attribute), branches (each representing the attribute value), and leaves (each representing a soil property). In this study, we used an advanced version of the regression tree called Cubist (Rulequest Research, Sydney). It is essentially similar to regression tree, except that the leaves are in the form of a linear regression of the covariates. A training dataset is used to discover or exploit the unknown relationships between the predictor variables and the predicted variable. It is assumed that all the required information to establish soil predictions is contained in the data and can be extracted if a sufficient amount of training data that cover the whole covariate space can be collected (Dobos et al., 2006; Elnaggar, 2007).

Here, using the 173 soil profile sites and the full suite of auxiliary data—including the predicted maps of ECav and ECah—regression tree models were built for each of the standard depths i.e. for 0–15, 15–30, 30–60 and 60–100 cm. Cubist models were used to model the deterministic spatial trend of ECe at the grid spacing of 90 m.

A total of 138 (80%) point data was used for calibration of the models, while the remaining data were used for validation. We used three different criteria for evaluating the performance of the spatial prediction models of ECe, namely, mean error (ME), root mean square error (RMSE), and coefficient of determination (R^2) and are equated below as:

$$\mathrm{ME} = \frac{1}{n}\sum_{i=1}^{n}(O_i - P_i)$$

$$\mathrm{RMSE} = \sqrt{\frac{1}{n}\sum_{i=1}^{n}(O_i - P_i)^2}$$

$$R^2 = \left[\frac{\sum_{i=1}^{n}(O_i - O_{ave})(P_i - P_{ave})}{\sqrt{\sum_{i=1}^{n}(O_i - O_{ave})^2 (P_i - P_{ave})^2}}\right]^2$$

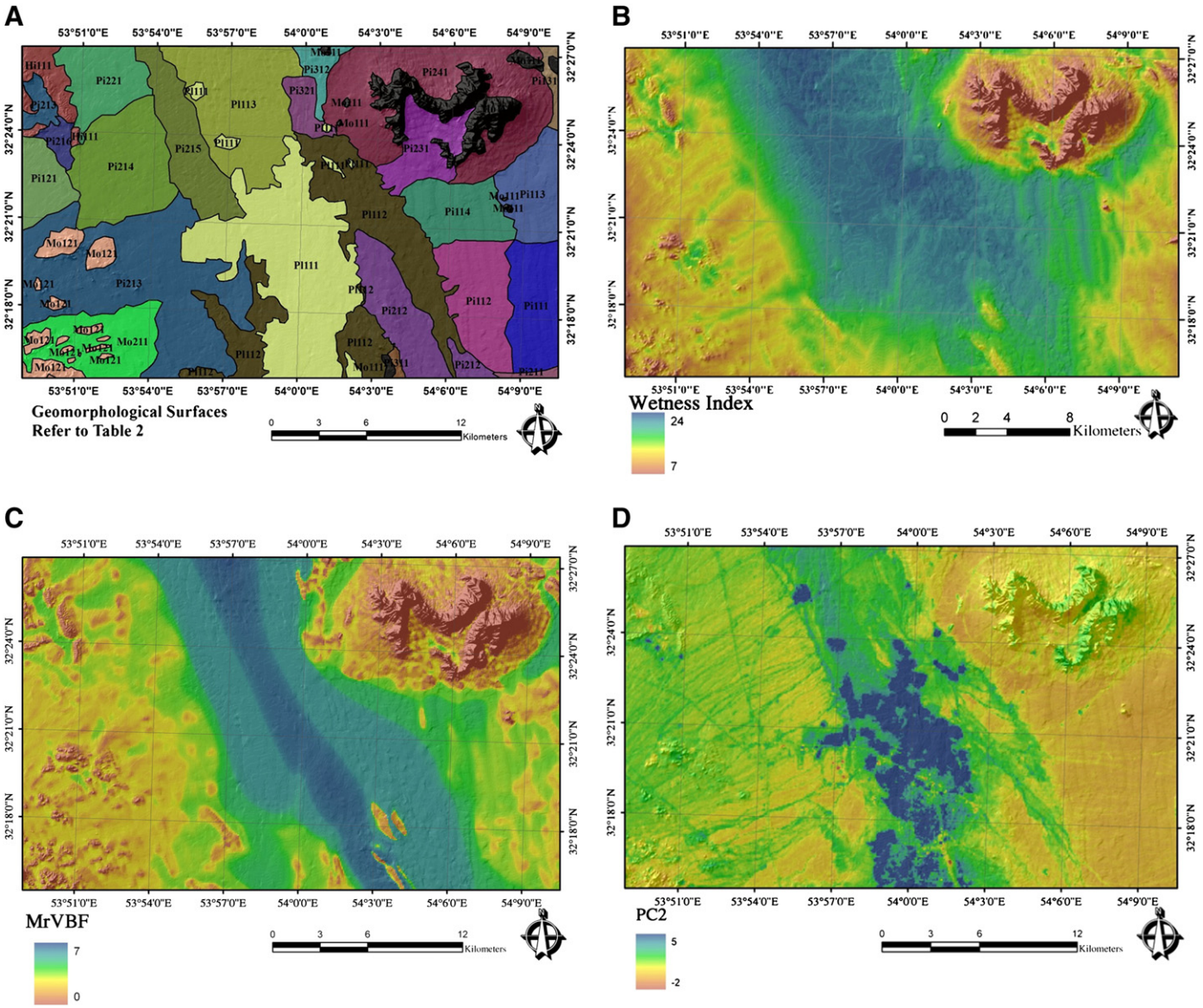

Fig. 3. Selection of auxiliary data of the Ardakan plain which included: (a) Geomorphology map (geomorphology codes refer to Table 2), (b) wetness index, (c) MrVBF, and (d) second principal component of the Landsat ETM^{+} image.

where P_i denotes the predicted values, O_i is the observed value, O_{ave} and P_{ave} shows the average of observed and predicted values, n is the number of data.

3. Results

3.1. Descriptive statistics of the ECe and ECa data

Summary statistics of soil salinity (ECe) at the different depths (to 1 m) and also ECa readings in both modes are presented in Table 3.

In general, 86% of soil samples have ECe above 4 dS m^{-1} and this suggests that soils in the study area are severely affected by salt. As the statistical results show, the median ECe levels in all four depth ranges are quite high, with values between 30 and 40 dS m^{-1} indicating that soils are considered as extremely saline. The soil salinity variations were similar in all four depth layers. The variations for soil salinity levels are very high with interquartile range between 48 and 108 dS m^{-1}, which indicate a broad range of values across the study area. Notably, ECe varied from 1 to 245 dS m^{-1} from top to the bottom of soil profiles. The high values of ECe are consistent with the values reported for samples taken from the Yazd province, which ranges from 0.48 to 171.3 dS m^{-1}. The soils here also contain a high concentration of gypsum (0–42.4 Cmol kg^{-1}) (Khorsandi and Yazdi, 2011). Likewise, the variation of ECa readings (1–340 mS m^{-1}) was also high in the vertical (ECav) and horizontal (ECah) modes. But to some extent, they are higher than the ECe measurements. It might be due to the device measured apparent electrical conductivity in larger volume soil, while electrical conductivity was measured in smaller soil samples taken from the genetic horizons only (Table 3).

Generally, soil samples found in the upper land have coarser texture (loamy sandy to sandy clay loamy) and low salinity, while soils in the lower part of the area are saline with finer textures (clay loam to clay). The samples with highest salinity level were located in the middle and northern of the study area.

3.2. Spatial distribution of auxiliary data

3.2.1. Terrain parameters

For prediction of soil salinity at the four depths, first we calculated terrain parameters from original DEM (i.e. 10 m pixel size) and its four levels of decomposed (i.e. 20, 40, 80, and 160 m pixel sizes). Then we compared the original DEM and its four levels of decomposed terrain

Table 2
Geomorphology map hierarchy and the major soil sub-great group per geomorphological surface.

Major sub-great group soil observed	Code	Geomorphological surface	Lithology	Landform	Landscape
Typic Torriorthents	Mo111	Rock outcrop	Dolomite-limestone	Dissected ridge	Mountain
Typic Torriorthents	Mo121	Rock outcrop	Grey to green andesitic, and limestone	Rock outcrop	
Typic Torriorthents	Mo211	Eroded surface	Eroded calcareous and dark shale	Rock pediment	
Typic Haplogypsids	Hi111	Dendrite drainage system with high topography	Sandstone-gypsum	Eroded rock outcrop	Hill land
Typic Haplocalcids	Pl111	Soft clay flat, salty and cultivated	Fine and coarse alluvial sediments	Ardakan basin	Playa
Gypsic Haplosalids	Pl112	Clay flat, dense stream, salty			
Gypsic Haplosalids	Pl113	Clay flat, highly salty and wetness			
Gypsic Haplosalids	Pi111	Active fan, upper section,	Alluvium of limestone	Alluvial fan	Piedmont
Gypsic Haplosalids	Pi112	Active fan, lower section, salty			
Petrogypsic Haplosalids	Pi113	Active fan, upper section with more drainage system, desert pavement			
Petrogypsic Haplosalids	Pi114	Active fan, lower section with more drainage system, desert pavement			
Typic Calcigypsids	Pi121	Active fan, lower section	Alluvium of grey limestone with red sandstone at the base		
Typic Haplogypsids	Pi131	Active fan, lower section	Alluvium sandstone, shale and limestone		
Gypsic Haplosalids	Pi211	Upper section, high slope, dense drainage system	Alluvium of grey limestone with red sandstone at the base	Bajada	
Gypsic Haplosalids	Pi212	Lower section, high slop			
Typic Calcigypsids	Pi213	Upper section, coarse, salty			
Gypsic Haplosalids	Pi214	Upper section, parallel streams			
Typic Haplocalcids	Pi215	Lower section, new deposits			
Gypsic Haplosalids	Pi216	Cultivated bajada, salty			
Gypsic Haplosalids	Pi221	Upper section, coarse, salty	Alluvium of gypsum hill lands		
Typic Haplocalcids	Pi231	Coarse, calcareous	Alluvium of dolomite-limestone		
Typic Haplocalcids	Pi241	Coarse, with dense drainage network	Alluvium of dolomite-limestone		
Gypsic Haplosalids	Pi311	Flat and lower topography	Alluvium of siltstone, shale, sandstone, gypsum	Old bajada	
Gypsic Haplosalids	Pi312	Higher topography and deep streams			
Typic Haplogypsids	Pi321	Higher topography and deep streams, coarse	Alluvium of gypsum		

attribute layers to predict ECe. Our results showed that for prediction of the target variable (ECe), the decomposed data layer L_4 (nominal resolution of 160 m) produced the best model and could enhance prediction accuracy by about 23%, 21%, 19%, and 17% for the 0–15 cm, 15–30 cm, 30–60 cm, and 60–100 cm depth intervals, respectively.

Fig. 3b shows the spatial distribution of wetness index. The small values (<7) are generally associated with the mountainous area, the intermediate values (7–14) are associated with parts of the bajada landforms, and the larger values of wetness index (>14) is corresponded to playa landforms. This area showed high potential of accumulation of salty materials. In fact this part of the area is located at the outlet of Ardakan basin and, hence has received a significant amount of soluble materials washed out from the entire watershed. According to sources such as Moore et al. (1991) and Jafari et al. (2012), there is a high correlation between soil salinity and topographic wetness index. Spatial distribution of MrVBF (Fig. 3c) shows a similar spatial trend to topographic wetness index. For example, the lowest value of MrVBF is highly associated with some parts of the area having high to moderate elevation and low topographic wetness. The highest value was corresponded in middle part and this part of area could be potential zones of transport for soil material in excess water flow.

3.2.2. Remote sensing data

Principal component analysis on the Landsat ETM$^+$ images showed that the first three components (PC1, PC2 and PC3) represent 99% of the variation of the spectral band data. The first component defined 90% of image variation and the highest eigenvalue belonged to Band 2 covering the green range of spectrum. Fig. 3d shows the spatial distribution of the second principal components (PC2) of the Landsat ETM$^+$ images. According to Fig. 3d, the largest values coincide with the irrigated areas and some of the vegetated areas in the central part of the study area, while the lowest values are associated with mountainous landform.

3.2.3. Apparent electrical conductivity

The ECa map for both vertical and horizontal mode was produced using the regression kriging approach. The evaluation of the prediction based on the training (80% of the data) and independent validation data set (20% of all data) is presented in Table 4. Both models show reasonable prediction with R^2 values around 0.49 on the validation dataset. The main predictors used in the model are wetness index (59%), geomorphology (48%), PC1 (31%), catchment aspect (17%), and valley depth (16%).

A map of the ECa in vertical mode is shown on Fig. 4a, and the horizontal mode in Fig. 4b. These maps clearly illustrate that there are two

Table 3
Descriptive statistics of soil ECe and ECa measurements.

Layer (cm)	Min	Max	Average	Std. Dev.	Q25[a]	Q50[a]	Q75[a]
ECe (0–15 cm) (dS m^{-1})	1	245.4	55.9	66.0	5.7	30.2	82.7
ECe (15–30 cm) (dS m^{-1})	1.3	238.6	64.2	66.8	7.4	33.8	115.3
ECe (30–60 cm) (dS m^{-1})	1	210.0	57.3	55.9	7.8	40.0	95.8
ECe (60–100 cm) (dS m^{-1})	1	231.9	40.7	41.1	9.7	30.4	57.4
ECa horizontal (mS m^{-1})	1	254	56.2	51.7	19.0	36.5	81.0
ECa vertical (mS m^{-1})	3	340	80.1	68.7	28.5	56.5	121.6

[a] Q25, Q50, and Q75 refer to the 25% quartile, median, and 75% quartile.

Table 4
Results of model evaluation criteria based on prediction and validation data sets for ECa readings in both vertical and horizontal modes.

	ME (mS/m)	RMSE (mS/m)	R^2
Prediction (n = 560)			
ECa horizontal	−0.12	24.95	0.69
ECa vertical	−1.03	30.78	0.75
Validation (n = 140)			
ECa horizontal	−2.23	29.64	0.48
ECa vertical	−1.07	37.74	0.49

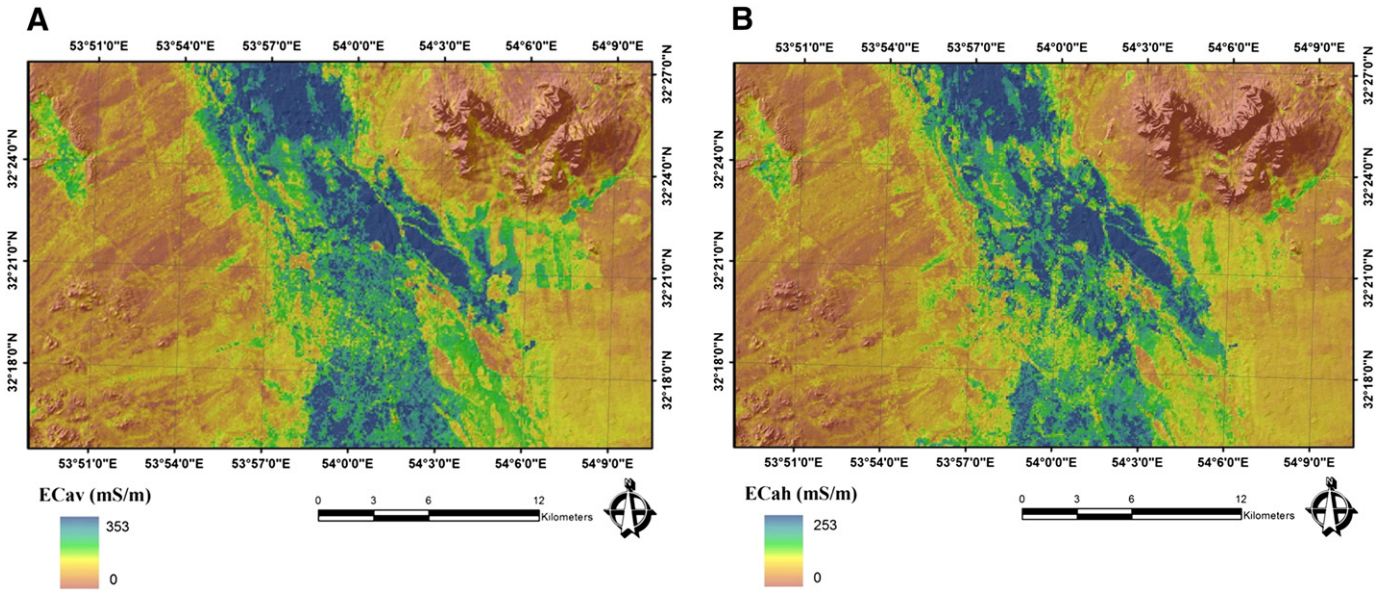

Fig. 4. (a) ECa in vertical mode and (b) ECa in horizontal mode.

distinct areas of high ECa values located in centre of region where the soil texture ranged from clays to loams, whereas areas of low ECa values were in east and west parts of the study area where the soil texture is coarser.

3.3. Relationship between ECe and ECa data

First we fitted linear regression models between ECa as independent variables and ECe as dependent variables for each depth. Consequently, four equations for the whole soil profile were derived (Table 5). This table shows that both vertical and horizontal measurements of ECa have a significant linear correlation with ECe for soils between 0 and 30 cm, whereas a lower correlation was found in 60–100 cm.

However the best model for soil surfaces only has an $R^2 = 0.67$, which is much lower when compared to other researchers' findings (Lesch et al., 2005; Slavich, 1990; Yao and Yang, 2010) who reported R^2 around 0.9. Therefore, we concluded that we cannot use the equations in Table 5 directly for the reconstruction the soil salinity profile across the study area. This might be attributed to the fact that ECa readings are influenced not only by soil salinity values but also by other factors such as texture, temperature and moisture content (Rhoades et al., 1990). Clay content in soils in some part of the study area particularly, in middle part and the north, exceeds 50% and, hence this might be one reason for lower correlation between apparent electrical conductivity and soil salinity levels in specified depths (Table 5). Another reason is the aridic condition, where the water content was below 5%. Low water content of the surface soil led lowering correlation between ECe and ECa readings (Bennett and George, 1995; McFarlane and Ryder, 1990). However, temperature has a smaller effect on our ECa values because the survey was conducted during summer period when average soil temperatures of the 1 metre profile are around 25 °C (Hendrickx et al., 1992).

Table 5
Regression relationships between ECa and measured ECe (n = 173).

			ECe = a + b.ECav + c.ECah	
Layer (cm)	a	b	c	R^2
ECe(0–15 cm) dS m^{-1}	1.5	0.43	0.49	0.67
ECe (15–30 cm) dS m^{-1}	10.3	0.39	0.50	0.61
ECe (30–60 cm) dS m^{-1}	22.8	0.62	−0.18	0.31
ECe (60–100 cm) dS m^{-1}	22.7	0.82	−0.75	0.14

3.4. Prediction of spatial distribution of ECe

We used digital maps of ECa (horizontal and vertical modes) along with other environmental variables to predict the spatial distribution of ECe at 4 depths. Validation results for the spatial prediction of ECe at each standard depth are shown in Table 6. According to this table, the evaluation of validation data sets resulted in R^2 values ranged from 0.78 to 0.11. These indicate much stronger predictions for the first layer of the soil profile in comparison to the last layer. The best prediction models were between 0–30 cm where the RMSE value ranged between 37.5 and 38.4 dS m^{-1}. The ME results showed that there was a very small positive bias (or underestimation) for predicted values in first standard depth (0–15 cm), whereas in the last depth (60–100 cm) there was a high positive bias. This could be the caused by the dry condition of the soil and low water content of the soil profiles. Added to this, variation of clay content (%) at the depth of 60–100 cm was very high (>57%).

We also run the Cubist model without including the ECa surfaces as predictors. Results showed that the prediction is worse with RMSE values that are 1.7 times higher for the 0–15 and 15–30 layers. The R^2 values are lower ranged from 0.36 to 0.08 for soil surface to the lowest depth (Table 6). So, these results convinced us (Tables 5 and 6) that although the ECa layers were predicted, they are a good representation of the ECa values, not just a combination of the other covariates. We

Table 6
Results of model evaluation criteria for ECe for the four standard depths based on a validation data set (n = 32) with all inputs (i.e. remote sensing, ECa, terrain parameters, and geomorphology), and without ECa covariates.

Layer (cm)	ME (dS/m)	RMSE (dS/m)	R^2
Models with all inputs including ECa			
ECe(0–15 cm) dS m^{-1}	0.99	37.52	0.78
ECe (15–30 cm) dS m^{-1}	−2.64	38.38	0.72
ECe (30–60 cm) dS m^{-1}	3.29	42.55	0.45
ECe (60–100 cm) dS m^{-1}	11.38	42.10	0.11
Models excluding ECa			
ECe(0–15 cm) dS m^{-1}	−1.64	64.08	0.36
ECe (15–30 cm) dS m^{-1}	−9.70	66.28	0.19
ECe (30–60 cm) dS m^{-1}	−1.92	56.79	0.02
ECe (60–100 cm) dS m^{-1}	7.13	42.93	0.08

should use ECa data combined with other environmental variables to map ECe.

The results also showed that some auxiliary data have more influence on the prediction of soil salinity in each depth. The most important auxiliary data used in the predictive models are presented in Fig. 5, showing the percentage of auxiliary data usage in each of the models. Generally ECav is a common variable for all standard depths as shown in Figs. 5a, b, and c. Meanwhile for 60–100 cm, topographic wetness index was the most important variable used in regression tree model (Fig. 5d).

We also calculated the contribution of each dominant factors used in the models and is illustrated in Fig. 6. For the 0–15 cm depth interval, remote sensing data had the highest influence on the model prediction followed by ECa, terrain attributes and geomorphology, whereas for the 60–100 cm depth interval, terrain attributes were the most predictive of ECe. Thus, we can imply that with increasing soil depth, the remote sensing data becomes less relevant, whereas the terrain parameters become more important.

The scatter plots of the measured against predicted ECe for each depth interval for the validation data sets are given in Fig. 7. These plots also indicate that the highest accuracy of estimation is for the top two standard depth intervals (Figs. 7a and b), whereas the lowest accuracy of estimation is for the 60–100 cm depth interval (Fig. 7d). This result implies that the sub-surface predictive models were non-optimal in defining a strong relationship between auxiliary data and

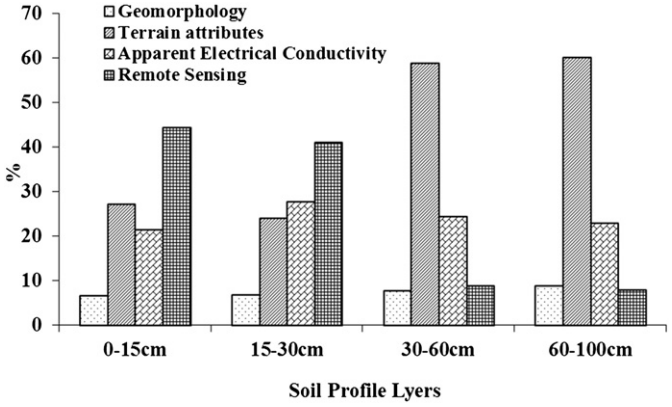

Fig. 6. The significance of each category of auxiliary data used in regression models in the four standard depths. Percentage represents the frequency of the auxiliary data used in the models.

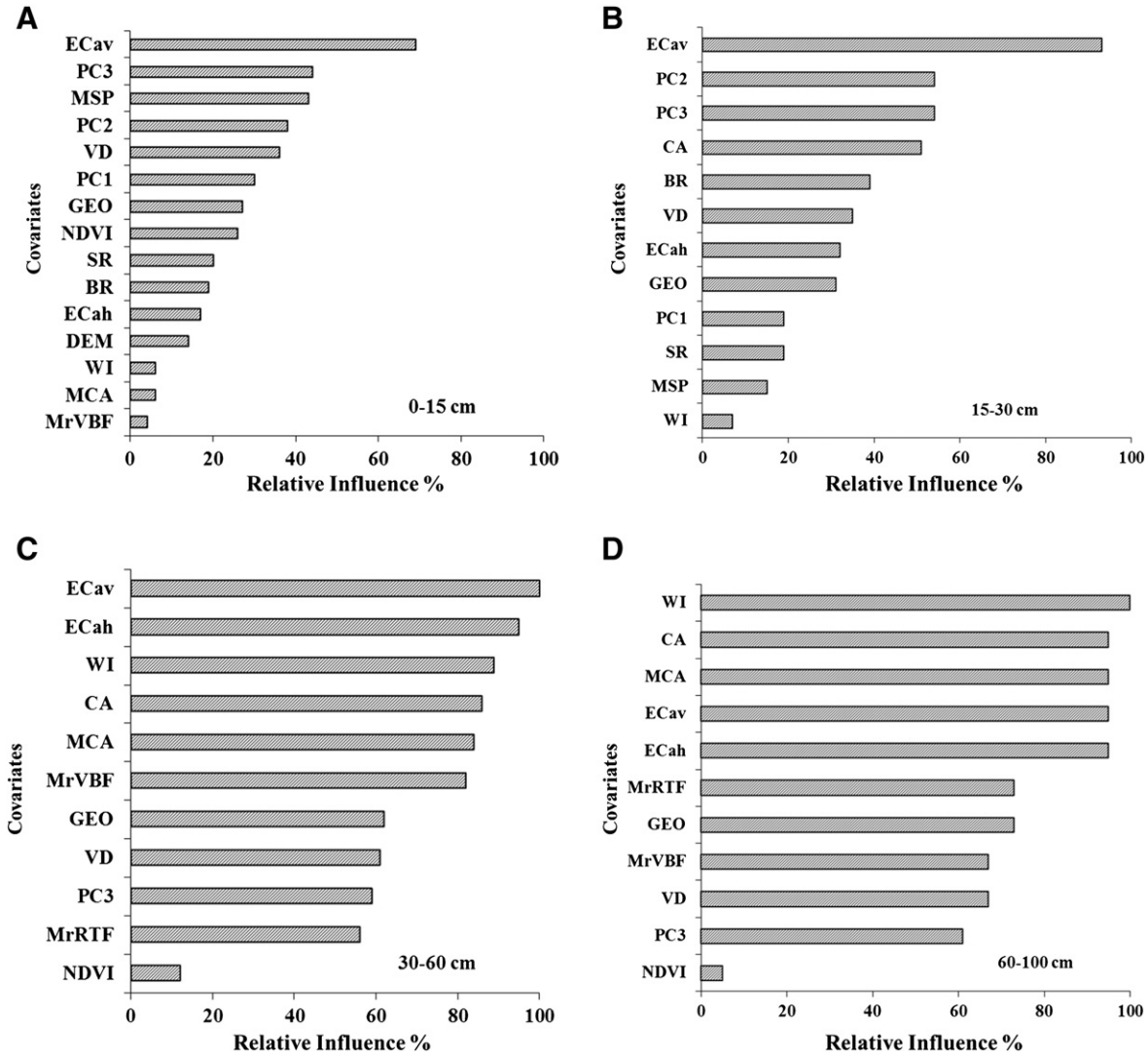

Fig. 5. The significance of each auxiliary data for prediction of ECe for the four standard depths: (a) 0–15 cm, (b) 15–30 cm, (c) 30–60 cm, and (d) 60–100 cm. Percentage represents the frequency of the auxiliary data used in the models. (WI: Wetness index, GEO: Geomorphology surfaces, PC: Principal component, MSP: Mid-slope position, NDVI: Normalized Difference Vegetation Index, VD: Valley depth, SR: Salinity ratio, BR: Brightness index, DEM: Elevation, MCA: Modified catchment area, MrVBF: Multi-resolution Valley Bottom Flatness Index, EM: Electromagnetic induction, MrRTF: Multi-resolution Ridge-top Flatness index, CA: Catchment aspect).

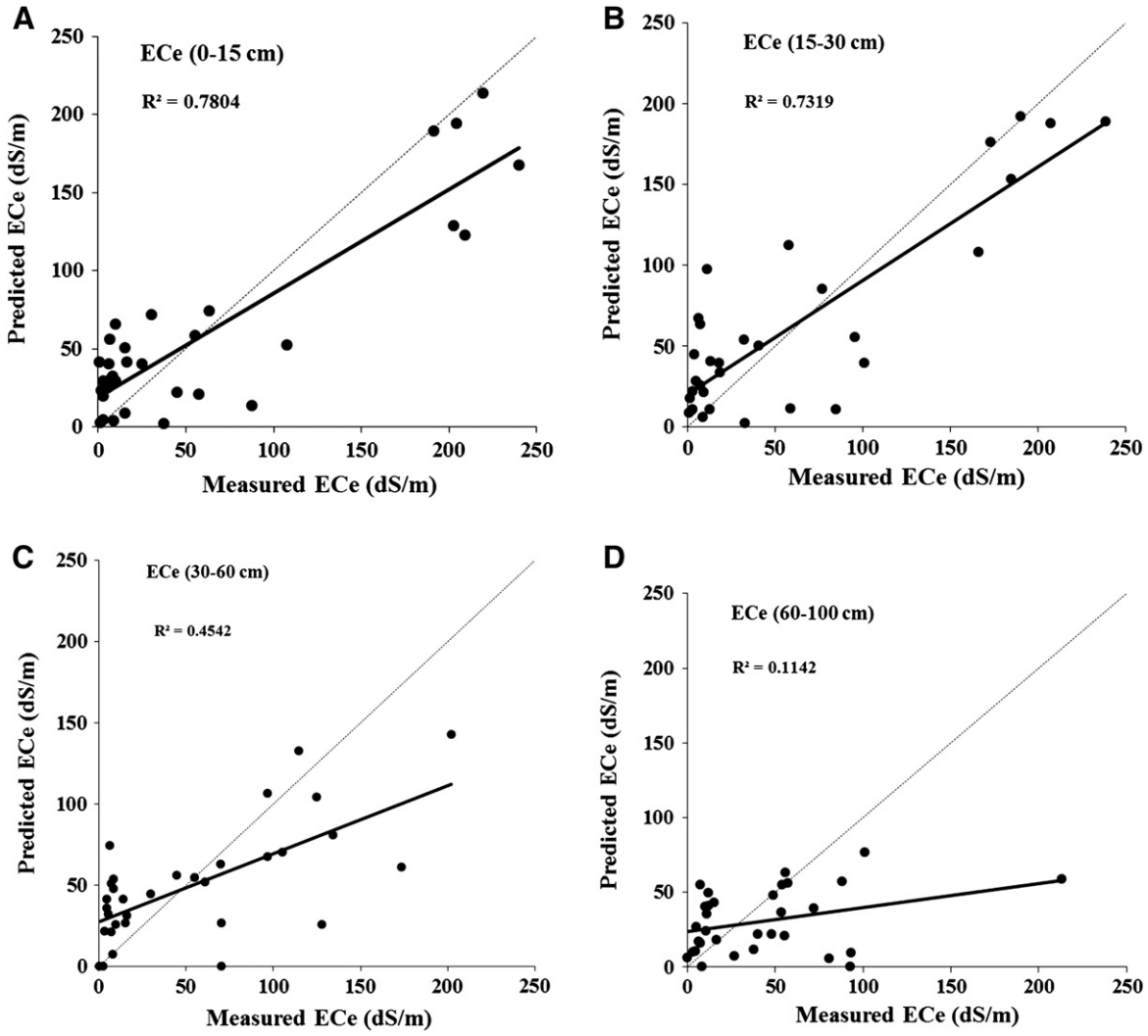

Fig. 7. Scatter plots of the measured versus predicted ECe: (a) 0–15 cm, (b) 15–30 cm, (c) 30–60 cm, and (d) 60–100 cm using regression trees through digital soil mapping approach based on validation data set.

ECe even with the help of EMI instrumentation. As an additional visual analysis of the validation, splines of the actual and predicted ECe values were fitted to four selected soil profiles and shown in Fig. 8. From these plots it is possible to get a sense that the vertical modelling of the ECe distribution with splines is feasible, in that the general vertical distribution of ECe is observed.

The regression rules defined by the Cubist models were applied to predict ECe across the study area at each depth interval (Fig. 9). As can be seen from these maps, the highest ECe can be found particularly at the 0–15 cm and 15–30 cm depth intervals and are located in the north and to the east of the study area. Areas of low salinity can be found in the north-west and north-east of the region.

Maps of the residuals (the difference between measured and predicted values) were also calculated to assess the uncertainty of the models. Results indicated that the error (residuals) is increasing with depth. The residual in the first layer (0–15 cm, Fig. 10a) is from −3 to 2, while the second layer (Fig. 10b) is from −15 to 10. The spatial distribution of soil salinity in of the third layer (30–60 cm, Fig. 9c) was similar to the first and second layers (Figs. 9a, b). The smallest values of soil salinity in this layer are generally associated in the west and the highest values of salinity are located in the north. The third layer showed the highest variation of error ranged from −31 to 48 (Fig. 10c). The spatial distribution in the bottom of soil profile (Fig. 9d) shows different trend and the regions with the highest salinity levels located in the west and fairly in the east of the study area.

4. Discussion

4.1. Auxiliary data used in predictive models

Our results (i.e. Fig. 5) demonstrated that one of the most important auxiliary data for prediction of electrical conductivity in the first three depth intervals (i.e. 0–15 cm, 15–30 cm and 30–60 cm), was the ECav layer. In contrast, the most important auxiliary data for prediction of soil salinity in 60–100 cm was topographic wetness index (Fig. 5d). Although the ECa surfaces were predicted, they were calibrated from a high number of ECa measurements and the accuracy of the prediction is quite good. Therefore they are a good representation of ECa values.

Akramkhanov et al. (2011) found that most terrain indices showed a low correlation with topsoil and bulk salinity, as their study area is quite flat. However, Moore et al. (1991) indicated a strong relationship between soil salinity and topographic wetness index. The results also suggested that the geomorphology map is another useful predictor for mapping soil salinity which might be due to the geomorphological surface that have formed recently and they have a good relationship with soil processes in the arid regions. This result is in line with other works, for example Scull et al. (2005) and Jafari et al. (2012) established that geomorphology is the best predictor for soil distribution in the desert ecosystem. In addition, remote sensing images are also useful predictors especially in the top soils (0–15 cm and 15–30 cm). Since most of the area was bare (Fig. 1d), hence the presence of salts at the

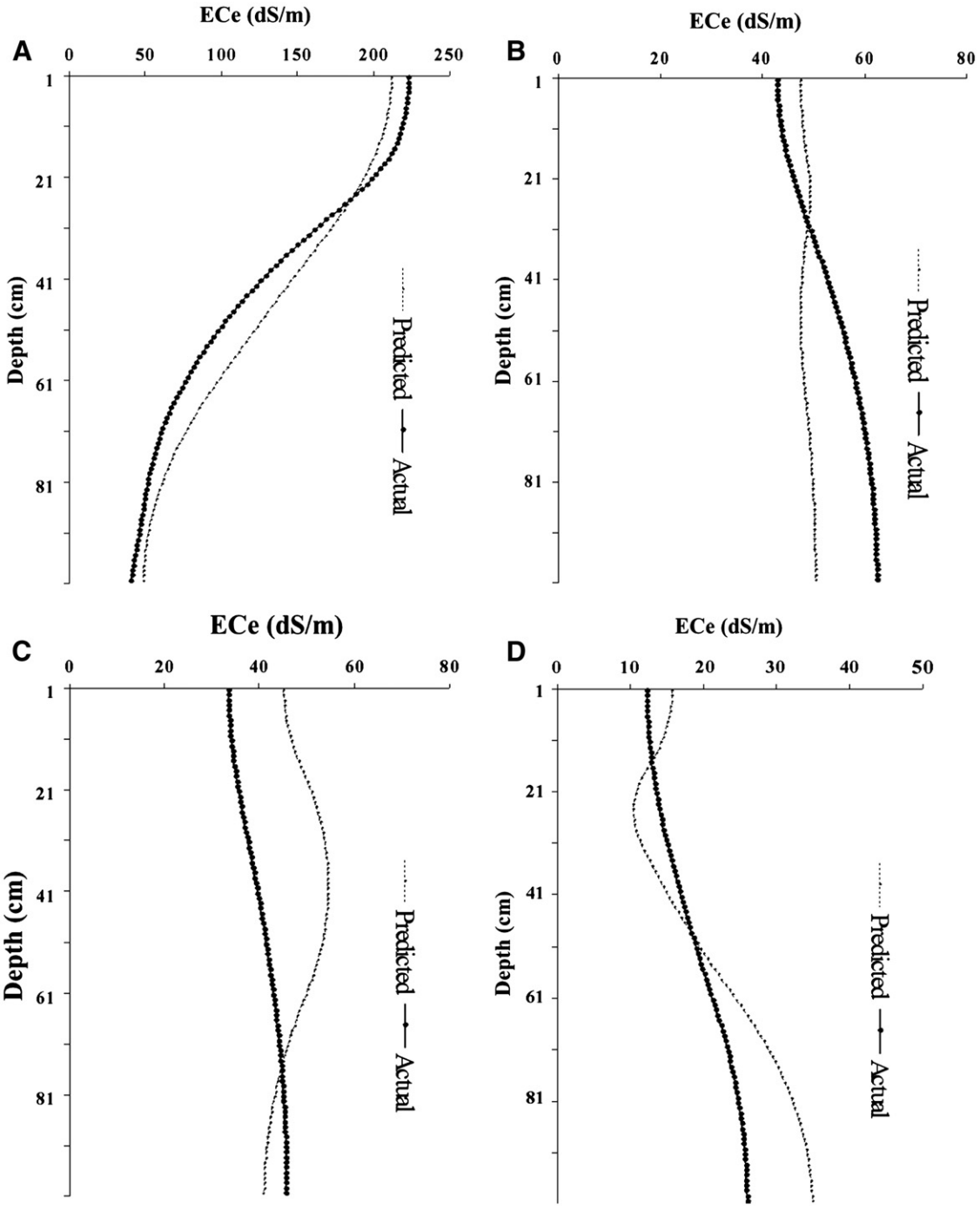

Fig. 8. Whole-profile representations of ECe distribution of observed values and corresponding predicted values. These profiles were selected from the validation dataset.

surface can easily be detected by principal components derived from the data (i.e. Landsat ETM$^+$). Metternicht and Zinck (2003) and similarly, Dwivedi and Sreenivas (1998) demonstrated that PCA of remotely sensed images is a useful approach to discriminate saline soils. Dehni and Lounis (2012) indicated that ETM images are helpful predictors for monitoring soil salinity.

4.2. Accuracy of the prediction models

With application of these auxiliary data, regression tree analysis predicted soil salinity values with ranging accuracy, dependent on the depth of spatial modelling—models performed better for the soil surface than at depth. These results agreed with findings of Ryan et al. (2000), Florinsky et al. (2002), Minasny et al. (2006) and Malone et al. (2009) who reported a decreasing accuracy of prediction with depth. These examples show that the covariates used cannot capture the subsurface variation. Nevertheless, for digital soil mapping, these results indicate a good accuracy, R^2 values over 70% are not very common and values of 50% or less are more common (Malone et al., 2009). In contrast, at deeper depth (60–100 cm), the accuracy is worse ($R^2 = 0.11$) even though the EMI instrument was supposed to have an effective depth of 0.75 and 1.5 m. This could be the caused by the dry condition of the soil and low water content of the soil profiles. Bennett and George (1995) and McFarlane and Ryder (1990) reported that moisture content

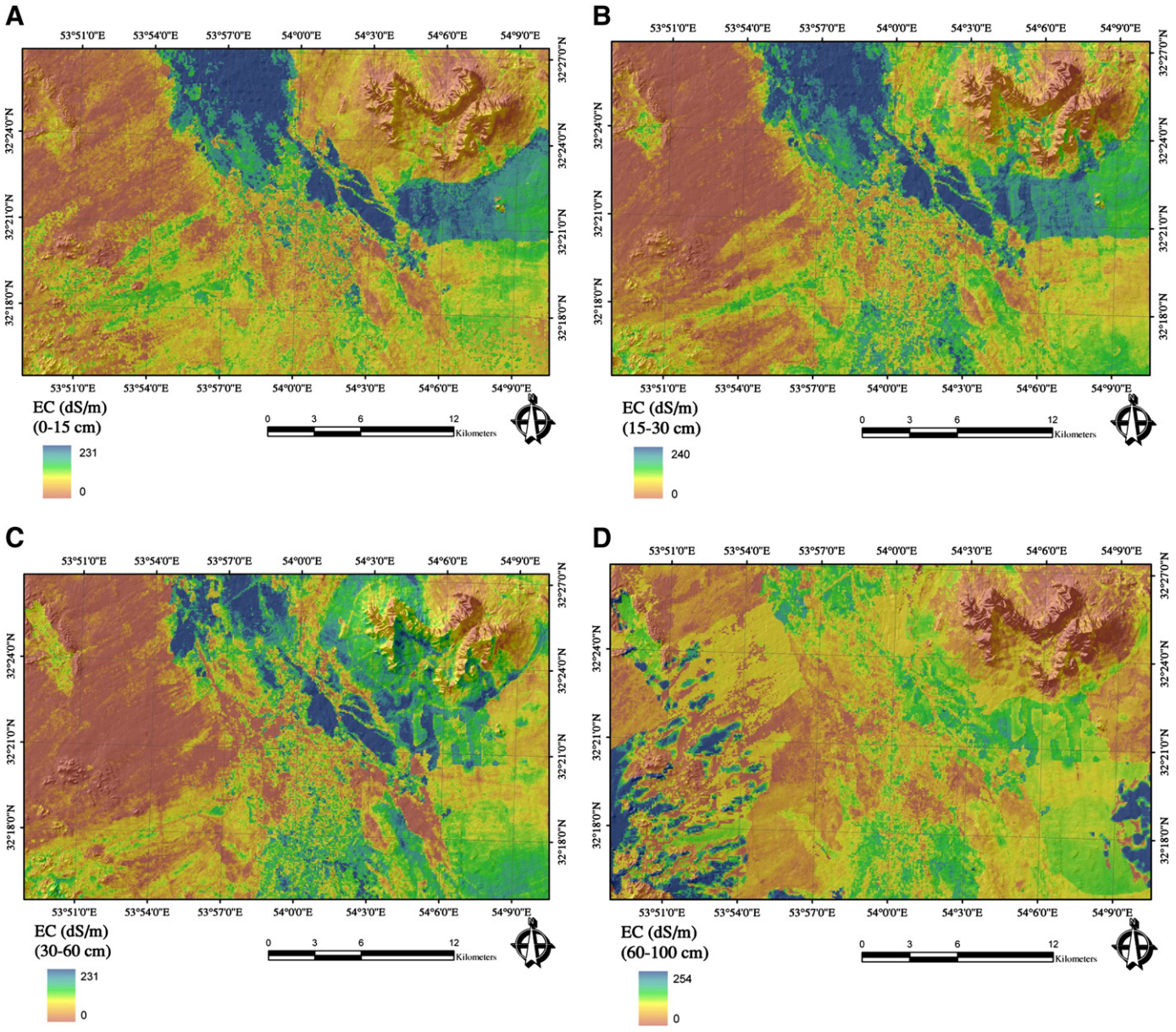

Fig. 9. Predicted maps of ECe (dS m^{-1}) to 1 m across the study area: (a) 0–15 cm, (b) 15–30 cm, (c) 30–60 cm, and (d) 60–100 cm.

has an important role in electromagnetic induction measurements. In addition, variation of clay content (%) at the depth of 60–100 cm was very high (>57%) and this could be another reason for lowering correlation. The low relief landscape in this study area made it difficult to model the topographic effect on soil salinity (Florinsky et al., 2002).

4.3. Spatial distribution of soil salinity

The salinity map (Fig. 9) shows that most of the saline soils are located in the lower part of the region, the playa landform. This is likely due to the playa having received more soluble salts washed out from upper areas. Added to this, the concavely shaped plain could help move ground water toward the north of the area in which the soils with highest ECe are found. In the north, the soil has a heavy texture and this might help the capillary movement of groundwater to the surface and, hence accumulation of salt in the surfaces. Although soils having a high ECe are not limited to the playa, Fig. 9 depicts some saline soils are also located in the east of the study area. In this area, there are salic and petrogypsic horizons with ECe levels more than 12 dS m^{-1}. Furthermore, Fig. 1c shows the poor vegetation cover in this landform which could be an indication of the presence of salic horizons.

Soil suitability assessment for the most arable crops needs this detailed information about the vertical and lateral variation of ECe. Consequently, a practicable and useful way to predict the lateral and vertical variation of soil salinity is from using combination of soil depth functions and digital soil mapping. Our results demonstrated that regression tree, and equal-area smoothing splines, as a composite DSM technique can be used to adequately model the lateral and vertical variations of soil salinity in central Iran.

5. Conclusions

We attempt in this study to investigate soil salinity variation (vertical and lateral) for a study area within Iran. Here, using soil data base and the full suite of auxiliary data— including the predicted maps of ECav and ECah, ETM^{+} images, geomorphology map, and

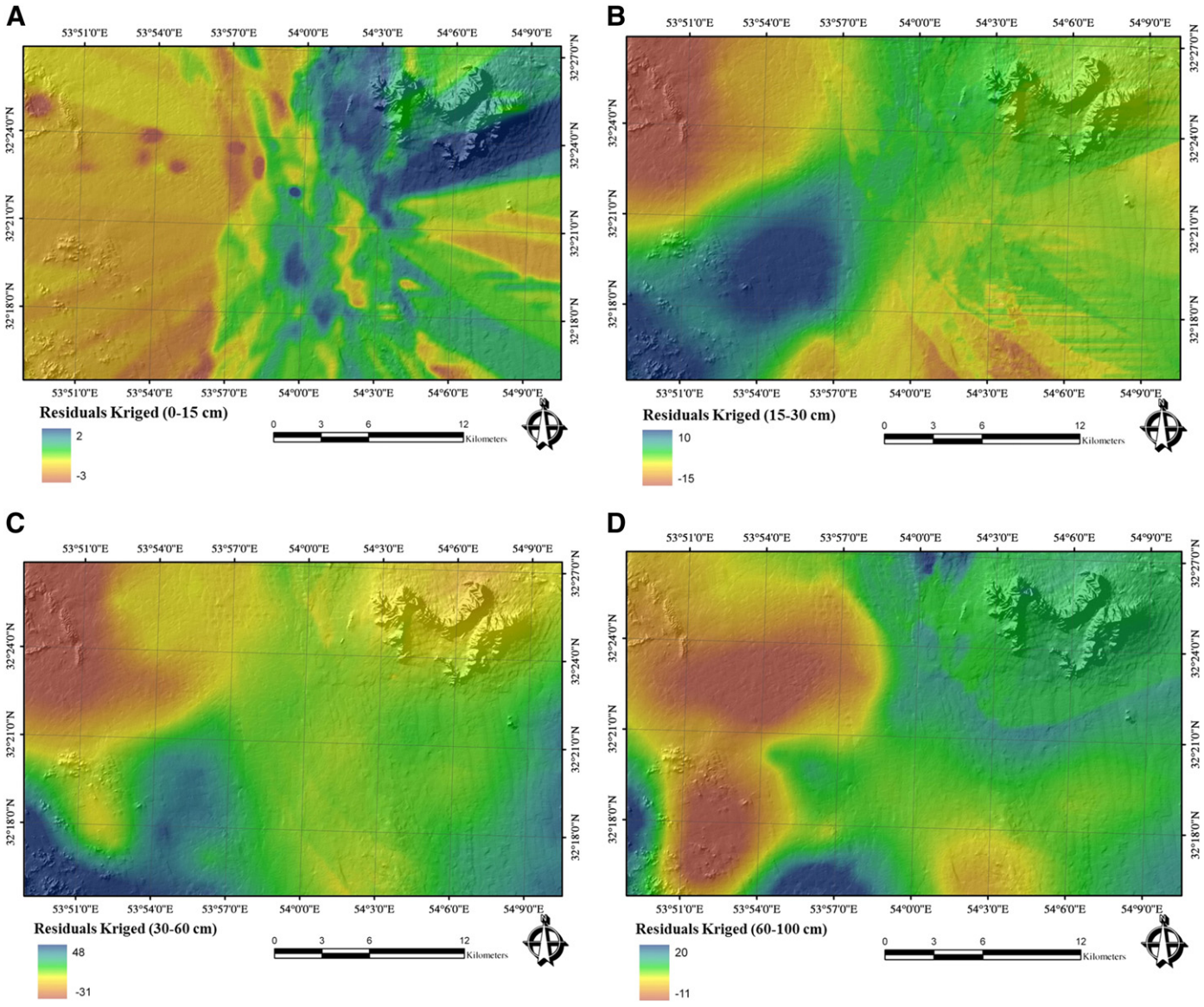

Fig. 10. Spatial distribution of residuals across the study area in four depths which included: (a) 0–15 cm, (b) 15–30 cm, (c) 30–60 cm, and (d) 60–100 cm. The prediction maps were generated by using local kriging.

terrain parameters—regression tree models were built for each of the standard depths i.e. for 0–15, 15–30, 30–60 and 60–100 cm depth intervals, respectively. The main conclusions that can be derived are:

- Our results confirmed that regression rule analysis (using Cubist) was a reliable approach that could be successfully used to prepare continuous soil salinity map.
- Remote sensing data (derived from such platforms as the Landsat ETM^+), apparent electrical conductivity, terrain parameters, and geomorphology units are the most useful predictors used for mapping of soil salinity in the study area. Results also confirmed that for the 0–15 cm depth interval, remote sensing data had the highest influence on the model prediction followed by ECa, terrain attributes and geomorphology, whereas for the 60–100 cm depth interval, terrain attributes were the most predictive of ECe. With increasing soil depth, the remote sensing data becomes less relevant, whereas the terrain parameters become more important.
- As a practicable and useful approach, spline functions are able to be used successfully in combination with regression rule models to predict continuous variation of soil salinity across the study area. However, the spatial prediction performed better for the soil surface than at depth, which shows that the current ancillary variables cannot capture subsurface variation.
- Fine-resolution electrical conductivity maps are useful for the many soil and environmental scientists and land managers in Iran (i.e. land degradation studies, mapping risk areas for wind erosion, soil quality assessments and soil erosion modelling). Therefore, we recommend the use of the approach applied at the study area to map the soil salinity in other parts of Iran.

References

Abdel-Kader, F.H., 2011. Digital soil mapping at pilot sites in northwest coast of Egypt: a multinomial logistic regression approach. The Egyptian Journal of Remote Sensing and Space Science 14, 29–40.

Akramkhanov, A., Vlek, P.L.G., 2012. The assessment of spatial distribution of soil salinity risk using neural network. Environmental Monitoring and Assessment 184, 2475–2485.

Akramkhanov, A., Martius, C., Park, S.J., Hendrickx, J.M.H., 2011. Environmental factors of spatial distribution of soil salinity on flat irrigated terrain. Geoderma 163, 55–62.

Alavi-Panah, S.K., Goossens, R., 2001. Relationship between the Landsat TM, MSS data and soil salinity. Journal of Agricultural Science and Technology 3, 21–31.

Andronikov, V.L., Dorbrolv'skiy, G.V., 1991. Theory and methods for the use of remote sensing in the study of soils. Mapping Sciences and Remote Sensing 28, 92–101.
Bennett, D.L., George, R.J., 1995. Using the EM38 to measure the effect of soil salinity on *Eucalyptus globulus* in south-western Australia. Agricultural Water Management 27, 69–86.
Bilgili, A.V., 2013. Spatial assessment of soil salinity in the Harran Plain using multiple kriging techniques. Environmental Monitoring and Assessment 185, 777–795.
Bishop, T.F.A., McBratney, A.B., Laslett, G.M., 1999. Modelling soil attribute depth functions with equal-area quadratic smoothing splines. Geoderma 91, 27–45.
Boettinger, J.L., Ramsey, R.D., Bodily, J.M., Cole, N.J., Kienast-Brown, S., Nield, S.J., Saunders, A.M., Stum, A.K., 2008. Landsat spectral data for digital soil mapping. In: Hartemink, A.E., McBratney, A.B., Mendonca-Santos, M.L. (Eds.), Digital Soil Mapping with Limited Data. Springer Science, Australia, pp. 193–203.
Bohner, J., Antonic, O., 2009. Land-surface parameters specific to topo-climatology. In: Hengl, T., Reuter, H.I. (Eds.), Geomorphometry: Concepts, Software, Applications. Elsevier, Amesterdam, pp. 192–226.
Bouaziz, M., Matschullat, J., Gloaguen, R., 2011. Improved remote sensing detection of soil salinity from a semi-arid climate in Northeast Brazil. Comptes Rendus Geosciences 343, 795–803.
Bui, E.N., Loughhead, A., Corner, R., 1999. Extracting soil-landscape rules from previous soil surveys. Australian Journal of Soil Research 37, 495–508.
National Cartographic Center, 2010. Research Institute of NCC, Tehran, Iran (www.ncc.org.ir).
Dehni, A., Lounis, M., 2012. Remote sensing techniques for salt affected soil mapping: application to the Oran region of Algeria. Procedia Engineering 33, 188–198.
Dobos, E., Carre, F., Hengl, T., Reuter, H.I., Toth, G., 2006. Digital soil mapping as a support to prediction of functional map. Digital Soil Mapping Working Group of the European Bureau Network. University of Miskolc, Miskolc-Egyetemváros, Hungary.
Douaoui, A.E.K., Nicolas, H., Walter, C., 2006. Detecting salinity hazards within a semiarid context by means of combining soil and remote-sensing data. Geoderma 134, 217–230.
Dwivedi, R.S., Sreenivas, K., 1998. Delineation of salt-affected soils and waterlogged areas in the Indo-Gangetic plains using IRS-1C LISS-III data. International Journal of Remote Sensing 14, 2739–2751.
Elnaggar, A.A., 2007. Development of predictive mapping techniques for soil survey and salinity mapping. (Doctoral dissertation, Oregon State University, Corvallis, Oregon). Retrieved from http://hdl.handle.net/1957/5754. 148 pp.
Evans, F.H., Caccetta, P.A., 2000. Broad-scale spatial prediction of areas at risk from dryland salinity. Cartography 29, 33–40.
Farifteh, J., Farshad, A., George, R.J., 2006. Assessing salt-affected soils using remote sensing, solute modelling, and geophysics. Geoderma 130, 191–206.
Florinsky, I.V., Eilers, R.G., Manning, G.R., Fuller, L.G., 2002. Prediction of soil properties by digital terrain modelling. Environmental Modelling & Software 17, 295–311.
Gallant, J.C., Dowling, T.I., 2003. A multiresolution index of valley bottom flatness for mapping depositional areas. Water Resources Research 39, 1347–1360.
Graps, A., 1995. An introduction to wavelets. IEEE Computational Science and Engineering 2, 50–61.
Grinand, C., Arrouays, D., Laroche, B., Martin, M.P., 2008. Extrapolating regional soil landscapes from an existing soil map: sampling intensity, validation procedures, and integration of spatial context. Geoderma 143, 180–190.
Hendrickx, J.M.H., Baerends, B., Raza, Z.I., Sadig, M., Haudhry, C.M.A., 1992. Soil salinity assessment by electromagnetic induction of irrigated land. Soil Science Society of American Journal 56, 1933–1941.
Hengl, T., Huvelink, G.B.M., Stein, A., 2004. A generic framework for spatial prediction of soil variables based on regression-kriging. Geoderma 120, 75–93.
Jafari, A., Finke, P.A., de Wauw, J.V., Ayoubi, S., Khademi, H., 2012. Spatial prediction of USDA — great soil groups in the arid Zarand region, Iran: comparing logistic regression approaches to predict diagnostic horizons and soil types. European Journal of Soil Science 63, 284–298.
Jenny, H., 1941. Factors of Soil Formation: A System of Quantitative Pedology. McGraw-Hill, New York (281 pp.).
Kempen, B., Brus, D.J., Stoorvogel, J.J., 2011. Three-dimensional mapping of soil organic matter content using soil type-specific depth functions. Geoderma 162, 107–123.
Khorsandi, F., Yazdi, F.A., 2011. Estimation of saturated paste extracts' electrical conductivity from 1:5 soil/water suspension and gypsum. Communications in Soil Science and Plant Analysis 42, 315–321.
Lacoste, M., Lemercier, B., Walter, C., 2011. Regional mapping of soil parent material by machine learning based on point data. Geomorphology 133, 90–99.
Lark, R.M., McBratney, A.B., 2002. Wavelet analysis. Chapter 1—soil sampling and statistical procedures. In: Dane, J.H., Topp, G.C. (Eds.), Methods of Soil Analysis. Part 4—Physical Methods. SSSA Book Series 5. Soil Science Society of America. Madison, Wisconsin, pp. 184–195.
Lark, R.M., Webster, R., 2004. Analysing soil variation in two dimensions with the discrete wavelet transform. European Journal of Soil Science 55, 777–797.
Lesch, S.M., Corwin, D.L., Robinson, D.A., 2005. Apparent soil electrical conductivity mapping as an agricultural management tool in arid zone soils. Computers and Electronics in Agriculture 46, 351–378.
Ließ, M., Glaser, B., Huwe, B., 2012. Uncertainty in the spatial prediction of soil texture: comparison of regression tree and random forest models. Geoderma 170, 70–79.
Malone, B.P., McBratney, A.B., Minasny, B., Laslett, G.M., 2009. Mapping continuous depth functions of soil carbon storage and available water capacity. Geoderma 154, 138–152.
Mathworks, 2010. Matlab version 7.0. The Mathworks Inc., Natick, MA.
McBratney, A.B., Mendonça-Santos, M.L., Minasny, B., 2003. On digital soil mapping. Geoderma 117, 3–52.
McFarlane, D.J., Ryder, A.T., 1990. Salinity and waterlogging on the Esperance Downs Research Station. Western Australian Department of Agriculture Division of Resource Management. Tech. Rep, vol.108.
McKenzie, N.J., Gessler, P.E., Ryan, P.J., O'Connell, D., 2000. The role of terrain analysis in soil mapping. In: Wilson, J., Gallant, J. (Eds.), Terrain Analysis: Principles And Applications. John Wiley and Sons, New York, pp. 245–265.
Mendonça-Santos, M.L., McBratney, A.B., Minasny, B., 2006. Soil prediction with spatially decomposed environmental factors. Digital Soil Mapping — An Introductory Perspective, 31 269–278.
Metternicht, G.I., Zinck, J.A., 1997. Spatial discrimination of salt- and sodium-affected soil surfaces. International Journal of Remote Sensing 18, 2571–2586.
Metternicht, G.I., Zinck, J.A., 2003. Remote sensing of soil salinity: potentials and constraints. Remote Sensing of Environment 85, 1–20.
Michot, D., Walter, C., Adam, I., Guéro, Y., 2013. Digital assessment of soil-salinity dynamics after a major flood in the Niger River valley. Geoderma 208, 193–204.
Minasny, B., McBratney, A.B., 2006. A conditioned Latin hypercube method for sampling in the presence of ancillary information. Computers & Geosciences 32, 1378–1388.
Minasny, B., McBratney, A.B., Whelan, B.M., 1999. Vesper Version 1.0. Australian Centre for Precision Agriculture. The University of Sydney, McMillan Building A05, NSW 2006 (http://www.usyd.edu.au/su/agric/acpa).
Minasny, B., McBratney, A.B., Mendonca-Santos, M.L., Odeh, I.O.A., Guyon, B., 2006. Prediction and digital mapping of soil carbon storage in the Lower Namoi Valley. Australian Journal of Soil Research 44, 233–244.
Mishra, U., Lal, R., Slater, B., Calhoun, F., Liu, D., Van Meirvenne, M., 2009. Predicting soil organic carbon stock using profile depth distribution functions and ordinary kriging. Soil Science Society of America Journal 73, 614–621.
Moore, I.D., Grayson, R.B., Ladson, A.R., 1991. Digital terrain modelling: a review of hydrological, geomorphological and biological applications. Hydrology Processing 5, 3–30.
Moran, C.J., Bui, E.N., 2002. Spatial data mining for enhanced soil map modeling. International Journal of Geographical Information Science 16, 533–549.
Nelson, D.W., Sommers, L.E., 1982. Total carbon, organic carbon, and organic matter, pp. 539–580. In: PageA, L., Miller, R.H., Keeney, D.R. (Eds.), Methods of Soil Analysis: Part II. American Society of Agronomy. Madison, WI, USA.
Nield, S.J., Boettnger, J.L., Ramsey, R.D., 2007. Digital mapping gypsic and nitric soil areas using Landsat ETM data. Soil Science Society of America Journal 71, 245–252.
Quinlan, J.R., 2001. Cubist: An Informal Tutorial. http://www.rulequest.com.
Rhoades, J.D., Shouse, P.J., Alves, W.J., Manteghi, N.A., Lesch, S.M., 1990. Determining soil salinity from soil electrical conductivity using different models and estimates. Soil Science Society of American Journal 54, 46–54.
Ryan, P.J., McKenzie, N.J., O'Connell, D., Loughhead, A.N., Leppert, P.M., Jacquier, D., Ashton, L., 2000. Integrating forest soils information across scales: spatial prediction of soil properties under Australian forests. Forest Ecology and Management 138, 139–157.
Scull, P., Franklin, J., Chadwick, O.A., 2005. The application of classification of tree analysis to soil type prediction in a desert landscape. Ecological Modelling 181, 1–15.
Sheng, J., Ma, L., Jiang, P., Li, B., Huang, F., Wu, H., 2010. Digital soil mapping to enable classification of the salt-affected soils in desert agro-ecological zones. Agricultural Water Management 97, 1944–1951.
Slavich, P.G., 1990. Determining ECa-depth profiles from electromagnetic induction measurements. Australian Journal of Soil Research 28, 453–463.
Soil Survey Staff, 2006. Keys to Soil Taxonomy, 10th ed. United States Department of Agriculture, Washington.
Sparks, D.L., Page, A.L., Helmke, P.A., Leoppert, R.H., Soltanpour, P.N., Tabatabai, M.A., Johnston, G.T., Summer, M.E., 1996. Methods of Soil Analysis, Soil Science Society of American Journal. Book Series No. 5. ASA and SSSA, Madison, Wisconsin.
Suarez, D.L., 1981. Relation between pHc and sodium adsorption ratio (SAR) and an alternative method of estimating SAR of soil or drainage waters. Soil Science Society of American Journal 45, 469–475.
Sun, W., Whelan, B.M., Minasny, B., McBratney, A.B., Whelan, B., 2012. Evaluation of a local regression kriging approach for mapping apparent electrical conductivity of soil (ECa) at high resolution. Journal of Plant Nutrition and Soil Science 175, 212–220.
Sun, Y., Cheng, Q., Lin, J., Schellberg, J., Schulze Lammers, P., 2013. Investigating soil physical properties and yield response in a grassland field using a dual-sensor penetrometer and EM38. Journal of Plant Nutrition and Soil Science 176, 209–216.
Toomanian, N., Jalalian, A., Khademi, H., Karimian Eghbal, M., Papritz, A., 2006. Pedodiversity and pedogenesis in Zayandeh-rud Valley, central Iran. Geomorphology 81, 376–393.
Triantafilis, J., Lesch, S.M., 2005. Mapping clay content variation using electromagnetic induction techniques. Computers and Electronics in Agriculture 46, 203–237.
Triantafilis, J., Odeh, I.O.A., McBratney, A.B., 2001. Five geostatistical models to predict soil salinity from electromagnetic induction data across irrigated cotton. Soil Science Society of America Journal 65, 869–878.
Vanwalleghem, T., Poesen, J., McBratney, A., Deckers, J., 2010. Spatial variability of soil horizon depth in natural loess-derived soils. Geoderma 157, 37–45.
Vasques, G.M., Grunwald, S., Comerford, N.B., Sickman, J.O., 2010. Regional modelling of soil carbon at multiple depths within a subtropical watershed. Geoderma 156, 326–336.
Yao, R., Yang, J., 2010. Quantitative evaluation of soil salinity and its spatial distribution using electromagnetic induction method. Agricultural Water Management 97, 1961–1970.